RESEARCH ARTICLE

Numerical Solution of Hybrid Nanofluid and Its Stability Over Permeable Wedge Sheet With Heat Transfer Analysis

AISHA M. ALQAHTANI[1], ZEESHAN[2], WARIS KHAN[3], FLORENTIN SMARANDACHE[4], NIDHAL BECHEIKH[5], ROOBAEA ALROOBAEA[6], AND TASEER MUHAMMAD[7]

[1]Department of Mathematical Sciences, College of Science, Princess Nourah bint Abdulrahman University, P. O. Box 84428, Riyadh 11671, Saudi Arabia
[2]Department of Mathematics and Statistics, Bacha Khan University Charsadda, Charsadda, Khyber Pakhtunkhwa 24420, Pakistan
[3]Department of Mathematics and Statistics, Hazara University Mansehra, Mansehra, Khyber Pakhtunkhwa 21300, Pakistan
[4]Mathematics, Physics, and Natural Science Division, The University of New Mexico, Gallup, NM 87301, USA
[5]Department of Chemical and Materials Engineering, Engineering College, Northern Border University, Arar 91431, Saudi Arabia
[6]Department of Computer Science, College of Computers and Information Technology, Taif University, Taif 21944, Saudi Arabia
[7]Department of Mathematics, College of Sciences, King Khalid University, Abha 61413, Saudi Arabia

Corresponding authors: Waris Khan (wariskhan758@yahoo.com) and Zeeshan (zeeshan@bkuc.edu.pk)

ABSTRACT The inclusion of nanoparticles has the potential to improve the thermal efficiency of the base fluid. The field of nanofluid (NF) dynamics has attracted important attention due to its extensive range of practical uses like fuel cells, solar energy, medication administration, heat transfer, microfabrication, coolant applications, and other related domains. The aim of this study is to scrutinize the impact of Lorentz force, thermal energy, joule heating, heat source and injection parameters, and Brownian and thermoporetic diffusions on the hybrid nanofluid over the moving wedge. The stability inquiry is reported for the existing work in order to confirm the stable solutions that make the study unique. Novelty of the existing work is to investigate the hybrid nanofluid flow and its stability. The nanoparticles MoS_2 and Ag are suspended in ethylene glycol and water used as host fluids. The numerical solution is obtained from the dimensionless first-order differential equations, which are achieved from the basic flow phenomena through similarity alteration variables. The influence of emerging factors on flow phenomena is reported via graphs. The positive eigenvalues report stable solutions, while the negative eigenvalues designate unstable solutions. It is perceived that due to Lorentz force, the rate of the fluid declines while the temperature inside the flow channel enhances. The velocity profile decreases while the temperature and concentration increase with increasing quantities of permeable factors. Similarly, the Forchheimer number causes to enhance the flow rate and decrease the heat and concentration outlines. The current analysis is validated by the published work.

INDEX TERMS Hybrid nanofluid, dual solutions, radiated heat flux, joule heating, moving wedge surface, porosity.

I. INTRODUCTION

By addition the nanoparticles, the host fluid's thermal efficiency may be raised. Because of its numerous practical applications—such as in fuel cells, solar energy, medication delivery, heat exchange, microfabrication, coolant, and other areas—nanofluid (NF) flow has received a lot of interest. The idea of a NF was initially presented by Choi [1] using suspended nanoparticles in the base fluid. It was determined that heat transmission in NF is developed than the base fluid. The chemical process occurring within the nanofluid along a horizontal tube was studied by Umavathi and Chamkha [2].

The associate editor coordinating the review of this manuscript and approving it for publication was Yilun Shang.

Analytical solution has been obtained. It was investigated that the chemical reaction factor destabilized the channel. The stability analysis was analyzed by Ketchate et al. [3] to investigate the non-Newtonian (NN) movement in the context of thermodynamic and magnetic fields. It was concluded that first solutions is sure while the second is unreliable. Puneeth et al. [4] examined the influence of bio-convection on the movement of a pseudoplastic NF over a revolving cone in the free stream numerically. It was reported that thermophoresis factor declines the concentration but improved the temperature distribution. Irfan et al. [5] explored the phenomenon of thermal relaxation in complex Carreau fluid with a heat source. Hussain et al. [6] explored the examination of NF motion influenced by velocity slip above a nonlinear stretched Riga surface with changing thickness and Joule heating. The mobility of the nanofluid in the cooling interaction was examined by Rafati et al. [7]. According to this analysis, the temperature significantly decreased, but the heat rate significantly increased. Razzaq and Farooq [8] explored the analysis of non-similar forced convection pertaining to the flow of Oldroyd-B fluid through a vertically stretched sheet. Numerical results have been obtained by using bvp4c approach. It was reported that temperature distribution declined with enhancing Prandtl number. Magnetohydrodynamics finds use in a number of fields, including nuclear electricity, electronic power plants, MHD engines, and electronic turbines. Razzaq and colleagues [9] conducted an investigation on the non-analogous resolution pertaining to the magnetized movement of a Maxwell nanofluid over a surface that is being exponentially extended. Cui et al. [10] investigated the thermal effect in bioconvection with chemically reaction over horizontal surface of Oldroyd-B fluid. Similalry, Lorentz force effect with entropy across the trapezoidal cavity comprising NFs was inspected by Mahmoudi et al. [11]. Their outcomes displayed that the addition of the NPs decreased the generation of entropy. Additionally, when the magnetic force became stronger, magnitude of entropy generation increased. Selimefendigal and Öztop [12] quantitatively inspected the magnetized hybrid conduction of NFs. This analysis reported that fluid velocity decrease with magnetic field. Öztop et al. [13] reported the phenomenon of mixed convection in a magnetohydrodynamic NF flow within wavy walls. The heat transmission level may be changed by growing or decreasing the proportion of NPs volume based on Hartmann and Richardson numbers.

Hybrid nanofluids, or HNFs, are frequently used to improve thermal performance and, consequently, heat rate transmission. Jan et al. [14] evaluated the behavior of MHD Sisko NF flow with viscous dissipations. It was reported that thermophoresis factor increases the concentration but Lewis number has inverse impact on concentration distribution.

Riaz et al. [15] reported computational analysis of heat transfer characteristics in a non-similar ternary HNF flow across a linearly extended sheet. In order to investigate HNF containing Ag-CuO, Hayat and Nadeem [16] used

water as the fundamental fluid throughout a spinning tube. A mathematical investigation of the impact of magnetic hydrodynamics on 3D HNF via extended sheeting was conducted by Devi and Devi [17]. It is originated that the melting effect is higher once the Fourier number varies from 0 and 0.5.

Chamkha et al. [18] used a horizontal tube to evaluate the efficiency of NF and HNF in order to assess the heat process. It was revealed that heat rate for HNF is higher than NF. Amala et al. [19] examined HNF through a moving vertical frame under the influence of heat sources and hall prospective. Analytical solution was obtained through Laplace transformation. For the same values of volume fraction, heat rate for HNF is higher than NF. Ghadikolaei [20] evaluated the enviroeconomic impact of solar PV cell cooling technique on carbon dioxide emissions reduction. Ghadikolaei [21] investigated how to increase the efficiency of photovoltaic solar panels using cooling technologies. Ghadikolaei and Gholinia [22] investigated 3D mixed convectional MHD movement of GO-MoS$_2$ HNF in H$_2$O-(CH$_2$OH) hybrid host liquid towards the impact of H2 bond. The same authors described the fantastic influence of H2 using convection-free motion of HNF in a permeable surface [23]. Similarly, same authors [24] considered the natural conduction movement of MHD caused by MoS$_2$-Ag nanomaterials embedded in C$_2$H$_6$O$_2$H$_2$O hybrid host fluid with thermal effect. Kumaran et al. [25] scrutinized the hydromagnetic driven convection movement of a Carreau NF across a wedge/plate with plate stagnation. Sudhagar et al. [26] considered the non-Darcy impressions of mixed convection NF across a wedge in a transparent medium. Gaffar et al. [27] studied mathematical exhibiting and outcomes for mixed convection BLFs of NF generated by a non-isothermal wedge. The system was solved numerically and it as concluded that Brownian motion has decreasing effect on concentration field.

In recent decades, researchers have paid close attention to the Falkner-Skan equation (FSE). Analytical and numerical procedures were used to produce the FSE's exact, almost accurate, and approximate findings. Mass transit is significantly impacted by a number of manufacturing processes, such as nuclear power plants, the cooling procedure, and polyester film, copper sheeting for cooling reasons, medical treatment strength, and aerospace engineering. Mohana and Kumar [28] investigated the consequences of Darcy-Forchheimer time-dependent 3D CdTe-C/H$_2$O HNF flow across a stretched sheet via convective transport of heat. Padmaja and Kumar [29] investigated the viscous dissipation and chemical response impacts on MHD NF flowing across a rotating channel using RK4 method. It was reported that Eckert number enhances the heat transfer rate. Hartree [30] provided closed-form solutions for FSE in a BLF. Yacob et al. [31] studied FSE over a fixed or dynamic wedge with heat analysis using NFF. Similarly, Alam et al. [32] investigated FSE in a magnetised nanofluid in a BLF through a moving wedge. Numerical consequences have been obtained and it is concluded that heat transportation rate enhances with FS parameter.

In view of the above literature review, there are few articles that focus on the motion of stable hybrid nanofluids through a moving wedge using the Falkner-Skan wedge flow framework in convective boundary conditions. The incorporation of nanoparticles has the potential to improve the thermal efficiency of the underlying fluid. The field of NF flow has garnered noteworthy attention due to its wide range of practical uses, including but not limited to fuel cells, solar energy, medication administration, heat transfer, microfabrication, coolant applications, and other related domains. The purpose of this study is to employ a modified Buongiorno structure to analyse the Falkner-Skan characteristics computationally for a non-homogeneous combination of ethylene glycol and water. Additionally, molybdenum disulfide and silver (Ag) tiny particles will be added through a movable transparent wedge sheet. The flow theory also takes into account the impacts of joule heating, Lorentz force, Brownian motion, thermophoresis features, and radiated thermal flow. The bvp4c method is employed to compute the complicated differential equations. For validation, the existing outcomes are equated with published outcomes and outstanding agreement is originated. The outcome of emerging features on heat, velocity, and concentration are revealed through graphs and tables. Since some factors exhibit multiple solutions, a stability evaluation is utilized for the stable solution. So, the novelty of the existing work is to investigate the HNF and its stability.

II. MATHEMATICAL ANALYSIS

Considering 2D time-independent movement over a porous movable wedge sheet with velocity $u_w(x) = U_w x^m/(1 - \alpha)$ and free-stream velocity $u_e(x) = \frac{U_e x^m}{1 - \alpha t}$ where α is constant. It is interesting to note that the inequality $U_w < 0$ indicates moving wedge and the equality $U_w = 0$ characterizes a static wedge. The flow geometry is portrayed in Figure 1. The basic flow equations also involve the key factors such as Lorentz force due to magnetic field, thermal radiations, heat rate, and Joule heating. The total wedge angle is $\Omega = \pi\beta$ where $\beta = \frac{2m}{m+1}$.
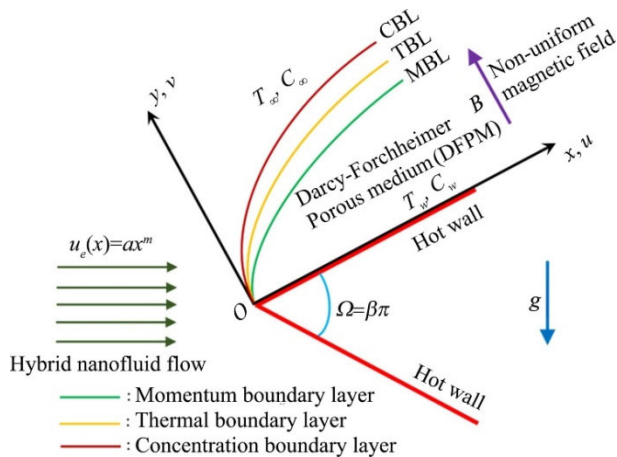

FIGURE 1. Schematic diagram.

Where, $m = 1$ represents the steady movement across the rotating wedge close to the stagnating zone, whereas $m = 0$ represents the flow through the moving wedge close to the plate. The $y-$ axis is vertical to the wedge and the $x-$axis is along to the movable wedge. The MBNM that configures the influence of thermophysical properties is the basis of the current HNF model.

The basic flows of equations are [35], [36], [37], [38], [39], [40]:

$$\frac{\partial u}{\partial x} + \frac{\partial v}{\partial y} = 0, \tag{1}$$

$$-\left(\frac{\sigma_{hnl}}{\rho_{hnl}}B^2 + \frac{\mu_{hnl}}{\rho_{hnl}K}\right)(u - u_e) - F\left(u^2 - u_e^2\right), \tag{2}$$

$$u\frac{\partial T}{\partial x} + v\frac{\partial T}{\partial y} = \frac{1}{(\rho c_p)_{hnl}}\left(k_{hnl}\frac{\partial^2 T}{\partial y^2} - \frac{\partial q_r}{\partial y}\right)$$

$$+ \frac{(\rho c_{c_n})_{np}}{(\rho c_p)_{hnl}}\left(D_B\frac{\partial C}{\partial y} + \frac{D_T}{T_\infty}\frac{\partial T}{\partial y}\right)\frac{\partial T}{\partial y} + \frac{\sigma_{hnl}B^2}{(\rho c_p)_{hnl}}u^2 \tag{3}$$

$$u\frac{\partial C}{\partial x} + v\frac{\partial C}{\partial y} = \frac{D_T}{T_\infty}\frac{\partial^2 T}{\partial y^2} + D_B\frac{\partial^2 C}{\partial y^2} \tag{4}$$

With

$$u(x) = \varepsilon u_w, v(x) = v_w, T(x) = T_w, C(x) = C_w \text{ at } y = 0,$$

$$u(x) \rightarrow u_e(x) = ax^m, T(x) \rightarrow T_\infty, C(x) \rightarrow C_\infty \text{ at } y \rightarrow \infty \tag{5}$$

In above equations u, v signify the velocities, T (temperature), and C (concentration), T_w (wall temperature), T_∞ (free-stream temperature), the wall NP volume fraction is represented by C_w while the free-stream volume Np is denoted by C_∞. Here, ρ is density, μ is the viscosity, , v denotes kinematic viscosity, and σ is the thermal conductivity. Radiated heat flux is denoted by q_r, D_T reports the thermal diffusion, and and D_B is Brownian diffusion coefficients. The inertia variable is $F = (F = \frac{C_d}{x\sqrt{K}})$ and porosity is given by the relation $K = K_0 x^{1-m}$, and varying magnetic field strength is $\vec{B} = B_0 x^{\frac{m-1}{2}}$. Also the partial volume fraction are denoted by χ_{M0S_2} and Ag_{M0S_2}. The thermo physical quantities for the present model are given in Tables 1 and 2.

Furthermore, the value of q_r in Eq. (3) is given by $q_r = -\frac{4\sigma^*}{3K^*}\frac{\partial T^4}{qy}$ (Rosseland approximation) [25]. Furthermore, when we describe the term T^4 as a linear function of T while disregarding the higher-order terms, become $T^4 = 4T_\infty^3 T - 3T_\infty^4$ so the equation becomes:

$$q_r = -\frac{16\sigma^2}{3\pi^*}T_\infty^3\frac{\partial I}{\partial y}$$

Presenting the alteration of variables, the scheme of equations (2)-(5) become while Eq. (1) satisfied identically [36], [37].

$$\frac{\eta}{y} = \left[\frac{a(m+1)}{2v_l}\right]^{\frac{1}{2}}x^{\frac{(m-1)}{2}}, \frac{\psi}{f(\eta)} = \left(\frac{2av_l}{m+1}\right)^{\frac{1}{2}}x^{\frac{(m+1)}{2}},$$

$$T = (T_w - T_\infty)\theta(\eta) + T_\infty, C$$

$$= (C_w - C_\infty)\phi(\eta) + C_\infty \tag{6}$$

TABLE 1. Thermophysical properties MoS_2, Ag and host fluids are [24].

Properties	Expressions
μ_{hnl}	$\mu_{hnl} = \dfrac{\mu_l}{\left[1 - (\chi_{Mos_2} + x_{Ag})\right]^{2.5}}$
ρ_{hnl}	$\rho_{hnl} = (1 - \chi)\rho_l + \chi_{MoS_2}\rho_{MoS_2} + \chi_{Ag}\rho_{Ag}$
(ρc_p)	$(\rho c_p)_{hnl} = (1 - \chi)(\rho c_p)_l +$ $\chi_{MoS_2}(\rho c_p)_{MoS_2} + \chi_{Ag}(\rho c_p)_{Ag}$
k_{hnl}	$k_{hnl} = \left[1 + \dfrac{3\chi(\chi_{Mos_2}k_{Mos_2} + \chi_{Ag}k_{Ag} - \chi k_l)}{(\chi_{Mos_2}k_{Mos_2} + \chi_{Ag}k_{Ag} + 2\chi k_l)} - \right]k_l$ $\chi(\chi_{Mos_2}k_{Mos_2} + \chi_{Ag}k_{Ag} - \chi k_l)k_l$
σ_{hnl}	$\sigma_{hnl} = \left[1 + \dfrac{3\chi(\chi_{Mos_2}\sigma_{Mos_2} + \chi_{Ag}\sigma_{Ag} - \chi\sigma_l)}{(\chi_{Mos_2}\sigma_{Mos_2} + \chi_{Ag}\sigma_{Ag} + 2\chi\sigma_l)} - \right]\sigma_l$ $\chi(\chi_{Mos_2}\sigma_{Mos_2} + \chi_{Ag}\sigma_{Ag} - \chi\sigma_l)$

TABLE 2. Thermophysical characteristics of $MoS_2 - Ag/C_2H_6O_2 - H_2O$ [24], [33].

Physical properties	Nanoparticles		Base fluid
	Silver	Molybdenum disulfide	$C_2H_6O_2 - H_2O$
Density (ρ)	10490	5060	1063.8
Specific heat (c_p)	235	397.21	3630
Thermal conductivity (k)	429	904.4	0.387
Electrical conductivity (σ)	6.30×10^7	2.09×10^4	9.75×10^{-4}
Pr	--	--	25.33

So, Eqs. (2)- (5) are distorted to:

$$f''' - \left(\frac{A_3 M^*}{A_1} + \frac{1}{P^*}\right)ff' + \frac{A_2}{A_1}f''$$
$$- \frac{A_2}{A_1}(\beta + F_P^*)f'^2 + \left(\frac{A_3 M^*}{A_1} + \frac{1}{P^*}\right) + \frac{A_2}{A_1}(\beta + F_p^*)$$
$$= 0, \qquad (7)$$

$$(A_4 + R_D)\theta'' + A_5 Pr\theta' + PrNb\theta'\phi'$$
$$+ 3\theta_r R_D \theta^2 + PrNt\theta'^2 + 3\theta_r R_D \theta\theta''$$
$$+ 6\theta_r^2 R_D \theta\theta'^2 + 3\theta_r^2 R_D \theta^2 \theta'' + 3\theta_r^3 R_D \theta^2 \theta'^2$$
$$+ \theta_r^3 R_D \theta^3 \theta'' + A_3 PrEcM^*f'^2 = 0, \qquad (8)$$

$$Nt\theta'' + Nb\phi'' + PrNbLef\phi' = 0. \qquad (9)$$

With

$$f(\eta) = S, f'(\eta) = \varepsilon, \phi(\eta) = 1, \phi(\eta) = 1, \text{ at } \eta = 0,$$
$$f'(\eta) \to, \theta(\eta) \to 0, \phi(\eta) \to 0, \text{ at } \eta \to \infty. \qquad (10)$$

The physical factors in above equations are:

$$Ec(\text{Eckert number}) = \frac{\rho_l u_c^2}{(\rho c_p)_l (T_w - T_\infty)},$$
$$Nb = \frac{\tau D_B (C_w - C_\infty)}{v_l},$$

$$Nt = \frac{\tau D_T (T_w - T_\infty)}{v_l T_\infty},$$
$$R_D = \frac{16\sigma^* T_\infty^3}{3k^* k_l}, \theta_w = \frac{T_w}{T_\infty},$$
$$Le(\text{Lewis numbar}) = \frac{k_l}{D_B (\rho c_p)_l},$$
$$Pr(\text{Prandtl number}) = \frac{(\rho c_p)_l v_l}{k_l},$$
$$F_P(\text{Forchheimernumber}) = \frac{2C_d}{\sqrt{K}}$$
$$M(\text{magnetic parameter}) = \frac{2\sigma_l B_0^2}{\rho_l a},$$
$$P(\text{porosity parameter}) = \frac{aK_0}{2v_l}.$$

These parameters are expressed as:

$$A_1 = \frac{\mu_{hnl}}{\mu_l}, A_2 = \frac{\rho_{hnl}}{\rho_l}, A_3 = \frac{\sigma_{hnl}}{\sigma_l}, A_4 = \frac{k_{hnl}}{k_l},$$
$$A_5 = \frac{(\rho c_p)_{hnl}}{(\rho c_p)_l}, \theta_r = \theta_w - 1, M^* = \frac{1}{m+1}M,$$
$$F_P^* = \frac{F_P}{m+1}, P^* = (m+1)P, \tau = \frac{(\rho c_p)_{np}}{(\rho c_p)_l}. \qquad (11)$$

The physical quantities of interest are given below:

$$C_{fr} = Re_x^{\frac{1}{2}} C_f = A_1 \sqrt{2m + 2} f''(0) \qquad (12)$$

$$Nu_r = Re_x^{-\frac{1}{2}} Nu_x = -\sqrt{\frac{m+1}{2}} \left(A_4 + R\theta_w^3 \right) \theta'(0), \quad (13)$$

$$Sh_r = Re_x^{-\frac{1}{T}} Sh_x = -\left(\frac{m+1}{2} \right)^{1/2} \phi'(0). \quad (14)$$

III. STABILITY ANALYSIS

Together with the shooting procedure, the resultant nonlinear system is elucidated computationally using the bvp4c technique. For the purposes of this investigation, stability evaluation is used since certain variables show dual solutions. Suction and injection lead to dual solutions. The approach used for stability reasons is explained in [33] and [34]. Following is the unsteady flow features (1)–(6).

$$\frac{\partial u}{\partial x} + \frac{\partial v}{\partial y} = 0, \quad (15)$$

$$\frac{\partial u}{\partial t} + u\frac{\partial u}{\partial x} + v\frac{\partial u}{\partial y} = u_e \frac{du_e}{dx} + \frac{\mu_{hnl}}{\rho_{hnl}} \frac{\partial^2 u}{\partial y^2}$$
$$- \left(\frac{\sigma_{hnl}}{\rho_{hnl}} B^2 + \frac{\mu_{hnl}}{\rho_{hnl} K} \right) (u - u_e) - F \left(u^2 - u_e^2 \right), \quad (16)$$

$$\frac{\partial T}{\partial t} + u\frac{\partial T}{\partial x} + v\frac{\partial T}{\partial y} = \frac{1}{(\rho c_p)_{hnl}} \left(k_{hnl} \frac{\partial^2 T}{\partial y^2} - \frac{\partial q_r}{\partial y} \right)$$
$$+ \frac{(\rho c_{c_n})_{np}}{(\rho c_p)_{hnl}} \left(D_B \frac{\partial C}{\partial y} + \frac{D_T}{T_\infty} \frac{\partial T}{\partial y} \right) \frac{\partial T}{\partial y} + \frac{\sigma_{hnl} B^2}{(\rho c_p)_{hnl}} u^2, \quad (17)$$

$$\frac{\partial C}{\partial t} + u\frac{\partial C}{\partial x} + v\frac{\partial C}{\partial y} = \frac{D_T}{T_\infty} \frac{\partial^2 T}{\partial y^2} + D_B \frac{\partial^2 C}{\partial y^2} \quad (18)$$

For stability purposes, the subsequent conversions are presented to convert the scheme to ODEs such as described via [33] and [34].

$$\frac{\eta}{y} = \left[\frac{a(m+1)}{2v_1} \right]^{\frac{1}{2}} x^{\frac{(m-1)}{2}} \frac{\psi}{f(\eta,\tau)} = \left(\frac{2av_1}{m+1} \right)^{\frac{1}{2}} x^{\frac{(m+1)}{2}},$$

$$T(x,\tau) = (T_w - T_\infty)\theta(\eta,\tau) + T_\infty,$$

$$C(x,\tau) = (C_w - C_\infty)\phi(\eta,\tau) + C_\infty, \tau = \frac{u_e x^{m-1}}{1-a}. \quad (19)$$

Eq.(20) in Eqs.(16)–(19), we get

$$\frac{\partial^3 f}{\partial \eta^3} - \left(\frac{A_3 M^*}{A_1} + \frac{1}{P^*} \right) f \frac{\partial f}{\partial \eta} + \frac{A_2}{A_1} \frac{\partial^2 f}{\partial \eta^2}$$
$$- \frac{A_2}{A_1} \left(\beta + F_P^* \right) \left(\frac{\partial f}{\partial \eta} \right)^2 + \left(\frac{A_3 M^*}{A_1} + \frac{1}{P^*} \right)$$
$$+ \frac{A_2}{A_1} \left(\beta + F_p^* \right) - (1 + a\tau) \frac{\partial^2 f}{\partial \eta \partial \tau} = 0, \quad (20)$$

$$(A_4 + R_D) \frac{\partial^2 \theta}{\partial \eta^2} + A_5 Pr \frac{\partial \theta}{\partial \eta} + PrNb \frac{\partial \theta}{\partial \eta} \frac{\partial \phi}{\partial \eta}$$
$$+ 3\theta_r R_D \theta^2 + PrNt \left(\frac{\partial \theta}{\partial \eta} \right)^2 + 3\theta_r R_D \theta \frac{\partial^2 \theta}{\partial \eta^2}$$
$$+ 6\theta_r^2 R_D \theta \left(\frac{\partial \theta}{\partial \eta} \right)^2 + 3\theta_r^2 R_D \theta^2 \frac{\partial^2 \theta}{\partial \eta^2} + 3\theta_r^3 R_D \theta^2 \left(\frac{\partial \theta}{\partial \eta} \right)^2$$
$$+ \theta_r^3 R_D \theta^3 \frac{\partial^2 \theta}{\partial \eta^2} + A_3 PrEcM^* \left(\frac{\partial F}{\partial \eta} \right)^2$$

$$- (1 + a\tau) \frac{\partial^2 \theta}{\partial \eta \partial \tau} = 0, \quad (21)$$

$$Nt \frac{\partial^2 \theta}{\partial \eta^2} + Nb \frac{\partial^2 \phi}{\partial \eta^2} + PrNbLef \frac{\partial \phi}{\partial \eta} - \frac{\partial \phi}{\partial \tau} = 0. \quad (22)$$

with

$$f(\eta,\tau) = S, \frac{\partial F}{\partial \eta}(\eta,\tau) = \varepsilon,$$

$$\phi(\eta,\tau) = 1, \phi(\eta,\tau) = 1 \text{ at } \eta = 0,$$

$$\frac{\partial F}{\partial \eta}(\eta,\tau) \to, \theta(\eta,\tau) \to 0, \phi(\eta,\tau) \to 0, \text{ at } \eta \to \infty. \quad (23)$$

By using the relation, the stability explanations are investigated for time-independent flow $f(\eta) = f_0(\eta), \theta(\eta) = \theta_0(\eta)$, and $\phi(\eta) = \phi_0(\eta)$ that satisfied the boundary constraints as described in [33] and [34].

$$f(\eta,\tau) = f_0(\eta) + e^{-\gamma\tau} J(\eta,\tau),$$

$$\theta(\eta,\tau) = \theta_0(\eta) + e^{-\gamma\tau} F(\eta,\tau),$$

$$\phi(\eta,\tau) = \phi_0(\eta) + e^{-\gamma\tau} G(\eta,\tau). \quad (24)$$

Unknown parameters, γ is the smallest eigenvalues. In view of (24), equations (20)-(23) become

$$J''' - \left(\frac{A_3 M^*}{A_1} + \frac{1}{P^*} \right) J' + \frac{A_2}{A_1} J'' - \frac{A_2}{A_1} \left(\beta + F_P^* \right) J'^2$$
$$+ \left(\frac{A_3 M^*}{A_1} + \frac{1}{P^*} \right) + \frac{A_2}{A_1} \left(\beta + F_p^* \right) + \gamma J - \frac{\partial J}{\partial \tau} = 0, \quad (25)$$

$$(A_4 + R_D) F'' + A_5 PrF' + PrNbF'G'$$
$$+ 3\theta_r R_D \theta_0^2 + PrNtF^2 + 3\theta_r R_D \theta_0 F''$$
$$+ 6\theta_{0r}^2 R_D \theta_0 F^2 + 3\theta_{0r}^2 R_D \theta_0^2 F'' + 3\theta_r^3 R_D \theta_0^2 F'^2$$
$$+ \theta_r^3 R_D \theta_0^3 F'' - \frac{\partial F}{\partial \tau} + A_3 PrECMM^* J'^2 + \gamma F = 0, \quad (26)$$

$$Nt\theta'' + Nb\phi'' + PrNbLef\phi'$$
$$+ \gamma G - \frac{\partial G}{\partial \tau} = 0. \quad (27)$$

The boundary conditions are

$$J(\eta,\tau) = S, J'(\eta,\tau) = \varepsilon, G(\eta,\tau) = 1,$$

$$F(\eta,\tau) = 1 \text{ at } \eta = 0,$$

$$J'(\eta,\tau) \to, F(\eta,\tau) \to 0, G(\eta,\tau) \to 0, \text{ at } \eta \to \infty. \quad (28)$$

So, equations (25)-(28) become

$$J''' - \left(\frac{A_3 M^*}{A_1} + \frac{1}{P^*} \right) J' + \frac{A_2}{A_1} J'' - \frac{A_2}{A_1} \left(\beta + F_P^* \right) J'^2$$
$$+ \left(\frac{A_3 M^*}{A_1} + \frac{1}{P^*} \right) + \frac{A_2}{A_1} \left(\beta + F_p^* \right) + \gamma J = 0, \quad (29)$$

$$(A_4 + R_D) F'' + A_5 PrF' + PrNbF'G'$$
$$+ 3\theta_r R_D \theta^2 + PrN tF'^2 + 3\theta_r R_D \theta F''$$
$$+ 6\theta_{0r}^2 R_D \theta F'^2 + 3\theta_r^2 R_D \theta^2 F'' + 3\theta_r^3 R_D \theta^2 F'^2$$
$$+ \theta_r^3 R_D \theta^3 F'' + A_3 PrEcM^* J^2 + \gamma F = 0, \quad (30)$$

$$NtF'' + NbG'' + PrNbLefG' + \gamma G = 0. \quad (31)$$

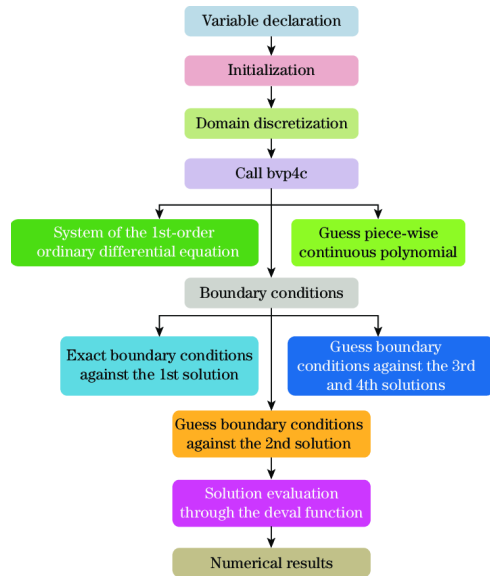**FIGURE 2.** Flow diagram of bvp4c. a. Dual solution presentation.

TABLE 3. Assessments of the present and available results when $F_P = M = 0, P_r = 0.73, R_D = M = E_C = 0.$

	$f''(0)$		$-\theta'(0)$	
m	Ref. [37]	Present study	Ref. [38]	Present study
0.0	0.46960	0.46841	0.42015	0.42113
0.1	0.50461	0.50441	0.42578	0.42578
0.2	0.56898	0.56863	0.43548	0.43525
0.3	0.65498	0.65472	0.44730	0.44711
0.5	0.73200	0.73212	0.45693	0.45673
0.8	0.80213	0.80204	0.46503	0.46501
1.0	0.92765	0.92752	0.47814	0.47805

With

$$J(\eta) = S, J'(\eta) = \varepsilon, G(\eta) = 1,$$
$$F(\eta) = 1 \text{ at } \eta = 0,$$
$$J'(\eta) \to, F(\eta) \to 0, G(\eta) \to 0, \text{ at } \eta \to \infty. \quad (32)$$

IV. NUMERICAL SOLUTIONS AND VALIDATION

The complex differential issues (7)–(9) related to the boundary limits (10) are computationally explained in Matlab by the bvp4c technique. A three-phase integration approach, as described. Collocation polynomials are used to achieve a homogeneous 4th-order resolution in an integration interval, similar to solution C1-continuous. In the second step, the time structure is divided into sub-intervals by applying a collocation approach to create a mesh. The mathematical system's solver ensures that a solution exists. To determine the error rate for each sub-interval, a solver is employed. If the necessary precision is not achieved, the process is carried out again using a modified mesh. The process chart for the bvp4c approach is shown in Figure 2. The present study is validtaed through the available outcomes and excellent settlement is found as illustrated in Table 1. With a tolerance of 10^{-9}, the results are said to be quite accurate and boundary condition $\eta \to \infty$ is taken as $\eta = 7$ and shows good convergence.

V. RESULTS AND DISCUSSION

PDEs are used to construct a mathematical framework for the non-homogeneous combination of 50% water and 50% ethylene glycol, along with the inclusion of molybdenum disulfide (MoS2) and silver (Ag) nanomaterials. In order to examine the features of Falkner-Skan features, the PDEs are transformed into a dimensionless set of equations with respect to nonlinear ordinary differential equations and computationally calculated using bvp4c over a moving permeable wedge sheet adopting the modified Buongiorno framework.

The influence of joule heating, suction/injection, magnetic field, thermophoresis characteristics, Brownian motion, and radiated heat flux on the flow characteristics are elaborated through graphs and tables. Together with the shooting procedure, the subsequent nonlinear differential system is elucidated computationally exhausting the bvp4c method. As demonstrated in Section IV, the reported results are verified with established results. For particular physical variables, dual solutions arise because of suctions or injections. As a result, the stability exploration is applied, as demonstrated in Section III. The bvp4c method is used to numerically solve the transformed equations (29)–(32) and fixed the parameters values as $p = 0.1, R_d = 0.2, F_p = 0.1, N_b = 0.3, N_t = 0.1,$ and $Le = 1.1$. These values are fixed in the whole investigation except when they are shown in graphs and tables.

Figure 3 provides a graphical representation of the dual solutions. According to Wiedman et al. [34] and Merkin [33], the suction parameter has an unstable solution for negative eigenvalues while being stable for the smallest positive eigenvalues. The crucial point is the point of convergence when the first and second branches come together. When there are multiple branches, the stability examination is significantly used for analyzing the stable branch. Figure 3 presents a visual depiction of the double solutions. The presence of negative eigenvalues indicates an unstable outcome, while the smallest positive eigenvalues indicate a stable solution. The critical point is that when the first and second branches converge. The smallest eigenvalues for different values of magnetic factor are also depicted in Table 4 when $Nb = 0.3, Nt = 0.4,$ $Le = 2, \theta_w = 1.2, P = 2, F_P = 2, R_D = 1.5, Ec = 0.1.$

Figures 4 and 5 characterize the impression of ϕ_{Ag} on the Skin Friction (SF) and Nusselt Number (NNb) about M,
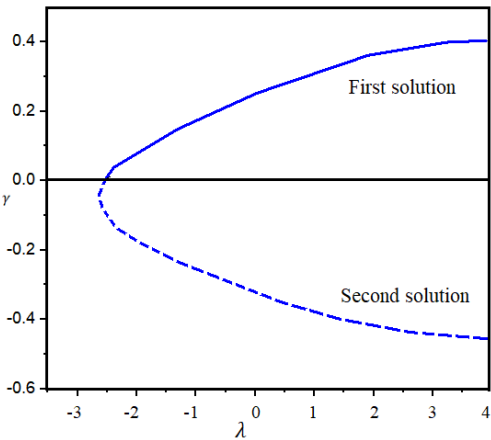
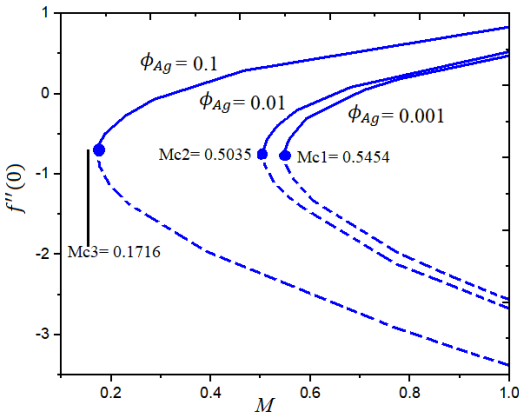**FIGURE 3.** Dual solution presentation.

TABLE 4. The first and second solutions for γ regarding several magnitudes of M when Nb = 0.3, Nt = 0.4, Le = 2, θ_w = 1.2, P = 2, F_P = 2, R_D = 1.5, Ec = 0.1.

M	γ	
	first solution	Second solutions
1	1.4023	−1.2358
0.8	1.1062	−1.0881
0.7	0.8505	−0.8245
0.5	0.6311	−0.6381
0.4	0.2025	−0.3273
0.2	0.0320	−0.0803
0.15	0.0061	−0.0002

FIGURE 4. Inspiration of ϕ_{Ag} on $f''(0)$.
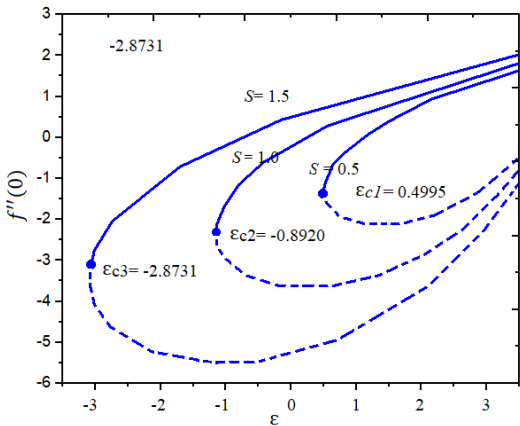
FIGURE 6. Inspiration of S on $f''(0)$.

FIGURE 5. Inspiration of ϕ_{Ag} on $-\theta'(0)$.

FIGURE 7. Inspiration of S on $-\theta'(0)$.

separately. Dual assessment takes place for ϕ_{Ag}. The hard line intelligences the first solution although the dotted line pinpoints the unstable solution. The critical magnitudes for $\phi_{Ag} = 0.001, 0, 01$, and $\phi_{Ag} = 0.1$ are $M_{c1} = 0.5454$, $M_{c2} = 0.5035$, and $M_{c1} = 0.1716$, correspondingly. It is worth mentioning at this point that SF boosts with increasing magnitudes of ϕ_{Ag} in the stable solution whereas diminishing in the unstable solution, as shown in Figure 4. Moreover, the

heat level drops for the stable solution however increasing for unstable solution. The relation between the free stream velocity ε and the suction on the SF as well as NNb is shown in Figures 6 and 7, correspondingly. The point which connects the first and second solutions with respect to the ε and S are $\varepsilon_{c1} = 0.4995$, $\varepsilon_{c2} = -0.8920$, and $\varepsilon_{c3} = -2.8731$ regarding to the suction $S = 0.5, 1.0$, and 1.5, respectively. It is investigated that the SF and NNb are increasing function of
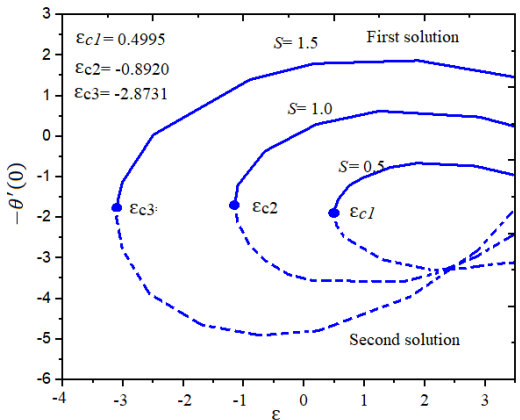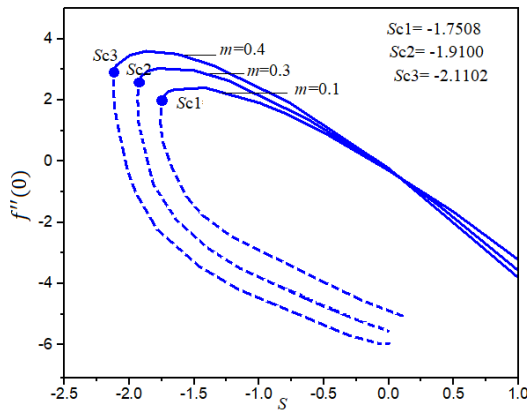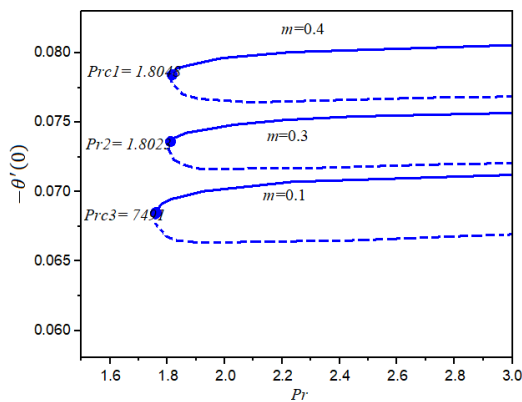
FIGURE 8. Inspiration of m on $f''(0)$.

FIGURE 9. Inspiration of m on $-\theta'(0)$.

ε and S, in the stable branch but decreasing in the unstable branch. In Figure 7 it is noteworthy to footnote that double manifestation arises in the unstable branch. In the domain $-3 \leq \varepsilon < 2$, deterioration performance is perceived for the NNb whereas in the interval $2 \leq \varepsilon \leq 3$ growing actions is recounted. Moreover, the impression of rotational angle m on the SF with NNb is exhibited in Figures 8 and 9, respectively regarding S and Pr. It is remarkable to annotation here that as m is increased, the profiles of f'' (0) and $-\theta'(0)$ are sketched to be enhanced in the first branch, which gives excellent agreement with the results reported by Ibrahim and Tulu [27]. This examination demonstrations a 3.8% escalation in heat as m is improved. This examination evidenced that once m is boosted, the thermal productivity of the base fluid develops. Likewise, it is described that at $\varepsilon = 1.0$, the SF approaches zero i.e., f'' (0) = 0, owing to no frictional drag force on the sheet while heated convectively.

The stability analysis has been discussed in detail by sketching the above graphs. In the following graphs 9-17, the impact of physical factors such as, wedge surface parameter M, magnetic factor P, permeable factor, F_P Forchheimer number, R_d thermal factor parameter, Lewis number, Eckert number, Brownian motion factor, and thermophoresis factor on the dimensionless velocity, temperature, and concentration profiles are discussed in detail. Graphs 18 and 19, report
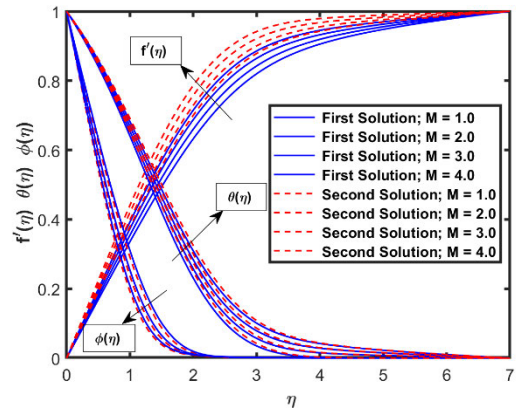

FIGURE 10. $f'(\eta), \theta(\eta)$, and $\phi(\eta)$ against M.

the variation of streamlines and isothermal flow for various values of magnetic and radiation factors. Similarly, Table 5 depicts the considerable effect of the nanoparticles on physical parameters of interest.

Figure 10 addresses the influence of magnetic factor M on $f'(\eta), \theta(\eta)$, and $\phi(\eta)$ profiles. It is significant to report here, that profiles $f'(\eta)$ and $\theta(\eta)$ are growing function of M whereas the concentration profile $\phi(\eta)$ decreases with increasing M. The quantities of the magnetic field impression denote the concentration of Lorentz forces. The aforementioned force is a resistive force which reduces the velocity of HNF. However, in the present study the fluid velocity raises with the growing magnitude of M. This conclusion a correlation with the outcomes of Ibrahim et al. [27]. It should be prominent that when $M = 0$, results in a TBL.

Figure 11 reveals the impact of m on $f'(\eta), \theta(\eta)$, and $\phi(\eta)$ distributions of the HNF. It is interesting to note here that as m is increased, the profiles of $f'(\eta)$, and $\theta(\eta)$, are sketched to be enhanced in the first branch and second branch, which gives excellent agreement with the results reported by Ibrahim and Tulu [27]. This exploration displays a 3.7% escalation in heat as m is improved. The investigations demonstrated that while m is boosted, the thermal proficiency of the base fluid enriches. Likewise, it is described that at $\varepsilon = 1.0$, the SF turn into zero i.e., $f''(0) = 0$, owing to no frictional drag force on the wedge surface when heated. The effects of m on $f'(\eta), \theta(\eta)$, and $\phi(\eta)$ profiles are shown in Figure 11. In this case, higher values of m fallouts in a reduction in the profiles $f'(\eta)$ while an escalation in $\theta(\eta)$ and $\phi(\eta)$ profiles are observed. The factor m is contrariwise related to β for $m < 1$. As the fluid flow slows, an escalation in the wedge angle causes a lessening in velocity. This result is consistent with Ibrahim and Tulu [27]. The variation of the variable P (permeability factor) on the profiles $f'(\eta), \theta(\eta)$, and $\phi(\eta)$ is reported in Figure 12. It is perceived that the velocity distribution $f'(\eta)$ decelerates as the quantities of P enhances. Physically, when the permeability variable grows, the fluid motion become slowly, this decays the momentum BLT significantly. Due to slow motion of the fluid over the isothermal wedge sheet the HNF heated significantly which increases the TBL.
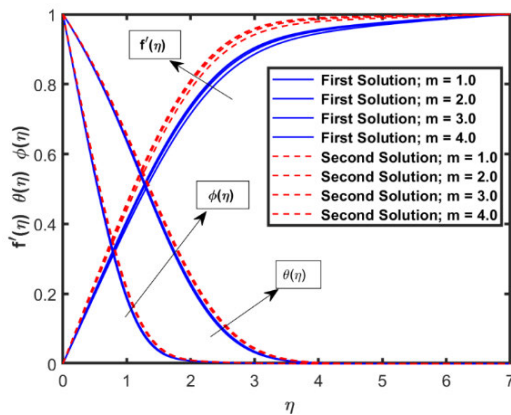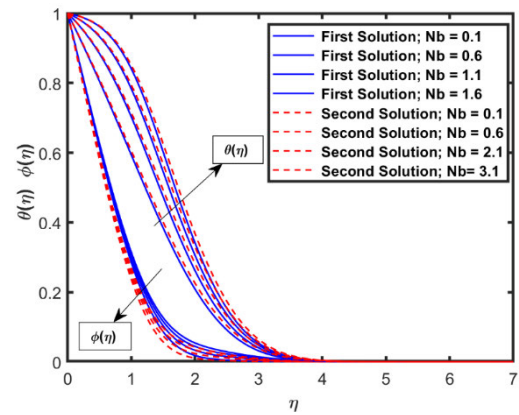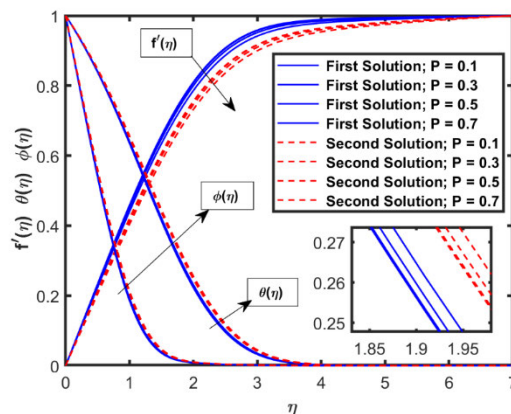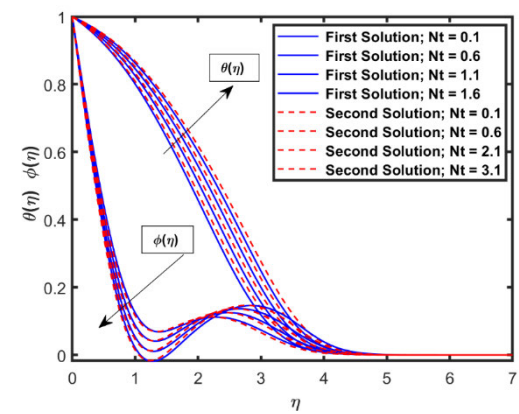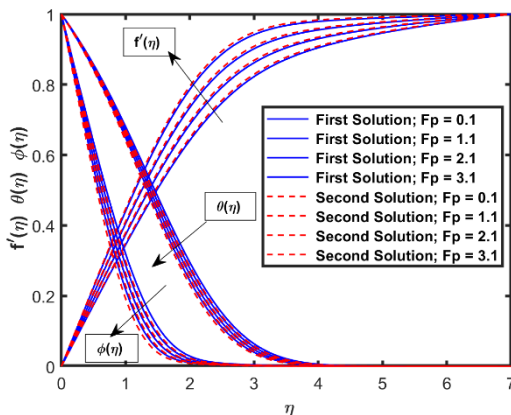
FIGURE 11. Variation of $f'(\eta), \theta(\eta)$, and $\phi(\eta)$ against m.

FIGURE 12. Variation of $f'(\eta), \theta(\eta)$, and $\phi(\eta)$ against P.

FIGURE 13. Variation of $f'(\eta), \theta(\eta)$, and $\phi(\eta)$ against Fp.

Figure 13 has been drafted to see the inspiration of F_p on dimensionless velocity, temperature and concentration profiles. Form this study dual branches have been observed. The fluid velocity enhances when the quantities of F_p is increased while opposed trend is detected for the $\theta(\eta)$, and $\phi(\eta)$ profiles. Comparing the three profiles, it is analyzed that variation is higher for the second branch than the first branch. This analysis is more visible from the velocity field.

The Brownian motion factor N_b effect on $\theta(\eta)$, and $\phi(\eta)$ is reported in Figure 14. Because of the random motion of the

FIGURE 14. Variation of $\theta(\eta)$, and $\phi(\eta)$ against N_b.

FIGURE 15. Variation of $\theta(\eta)$, and $\phi(\eta)$ against Nt.

tiny fluid molecules, the energy generated within the fluid which enriches the fluid temperature but the concentration decreases. Comparing the profiles of $\theta(\eta)$, and $\phi(\eta)$, the unstable solution is greater than the stable. The variation of $\theta(\eta)$ and $\phi(\eta)$ due to themophoresis factor N_t is shown in Figure 15. When N_t increases, due to thermophoresis mechanism the heated molecules are moved away from the hottest zone to the smallest zone which causes the inflation of the HNF temperature for both stable and unstable solutions. While, the concentration outlines decrease.

Figure 16 portrays the performance of $\theta(\eta)$, and $\phi(\eta)$ when the Le is augmented. It is significant to note that both profiles decline as the Le is increased. In physics point of view, when Le is increased, the mass diffusivity of the fluid decreases due to which thermal diffusivity enhances which decline the temperature and concentration. It is perceived that the increase in the first solution is more significant than the second one.

Joule heating characteristics can be expressed by the product of Ec and magnetic factor. Already, discussed in aforementioned graph (see Fig. 10) that as M is increased the temperature is improved. In the same way the effect of Ec on temperature is same. Similarly, thermal radiation R_d impact on the temperature field is directly proportional. As the quantities of R_d are enhanced the temperature inside the fluid increase and this increasing is higher for the second
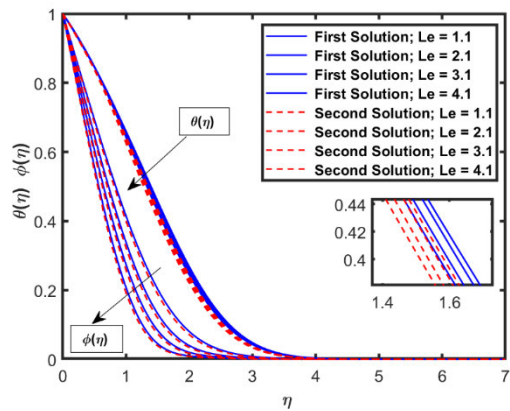
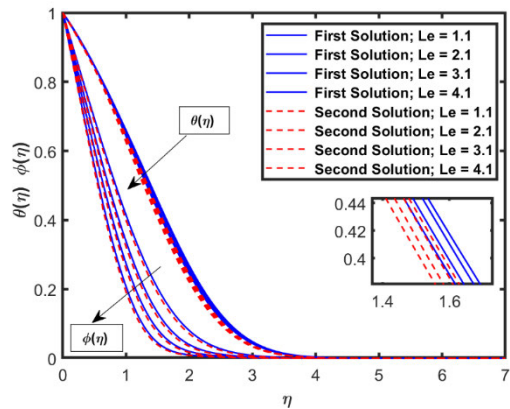**FIGURE 16.** Variation of $\theta(\eta)$, and $\phi(\eta)$ against Le.

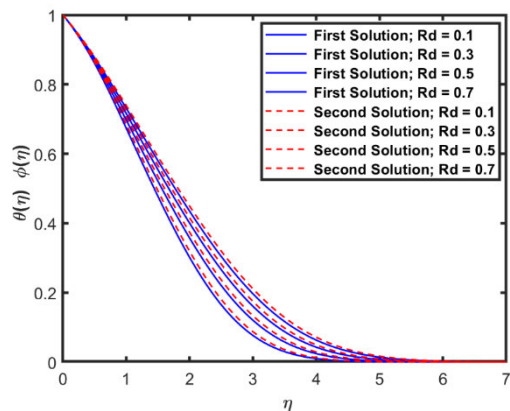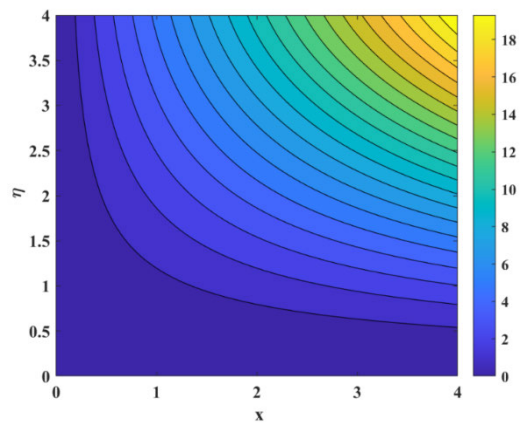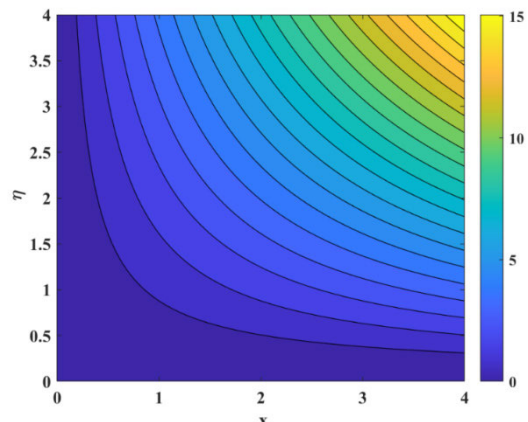**FIGURE 17.** Variation of $\theta(\eta)$, and $\phi(\eta)$ against Ec.

FIGURE 18. Variation of $\theta(\eta)$ and $\phi(\eta)$ against R_d.

FIGURE 19. (a). Streamlines for $M = 1.0$. (b). Streamlines for $M = 1.2$.

TABLE 5. Influence of χ_{MoS_2}, χ_{Ag} on C_{fr}, Nu_r, and Sh_r when $\chi = 0.20$, $m = \frac{1}{3}$, $M = 0.1$, $P = 2$, $F_P = 2$, $R_D = 1.5$, $Ec = 0.12$, $Nb = 0.3$, $Nt = 0.4$, $Le = 2$, $\theta_w = 1.2$.

Sh_r	E_f	E_h	E_m
1.24200675	--------	-------	-------
1.30510430	04.00%	0.560%	0.535%
1.32423336	9.7664%	1.200%	1.123%
1.36000460	15.157%	2.700%	2.574%
1.40301560	20.403%	4.077%	4.011%

χ_{MoS_2}	χ_{Ag}	C_{fr}	Nu_r
0.4	0.1	3.06202	0.11045
0.3	0.3	4.30085	0.11646
0.2	0.2	4.60022	0.12071
0.1	0.3	5.06307	0.21258
0.0	0.4	5.13507	0.13034

solution. When the radiation factor is improved, more heat is generated due to the radiation reaction in HNF which enhance the temperature inside the fluid.

Streamlines are designed for two dissimilar quantities of $M = 1.0$ and $M = 1.2$ as publicized in Figure 19 (a-b). For dissimilar quantities of M streamlines are dropped. The isothermal movement for the assumed model is reconnoitered in Figure 20 (a-b) by altered magnitudes of radiated parameter. It is publicized that as the magnitude of R_d upturns from $R_d = 0.2$ to $R_d = 1.2$, the contour plots of heat boosts. Table 5 shows the significance of MoS$_2$ and Ag on

the improvement rate E_f, E_h, and E_m of the physical quantities of interest C_{fr}, Nu_r, and Sh_r Additionally, it is shown that the related enhancement rates E_f, E_h, and E_m are significantly increased when the solid nanoparticles MoS2 are suspended in a volumetric percentage of solid nanomaterial Ag.
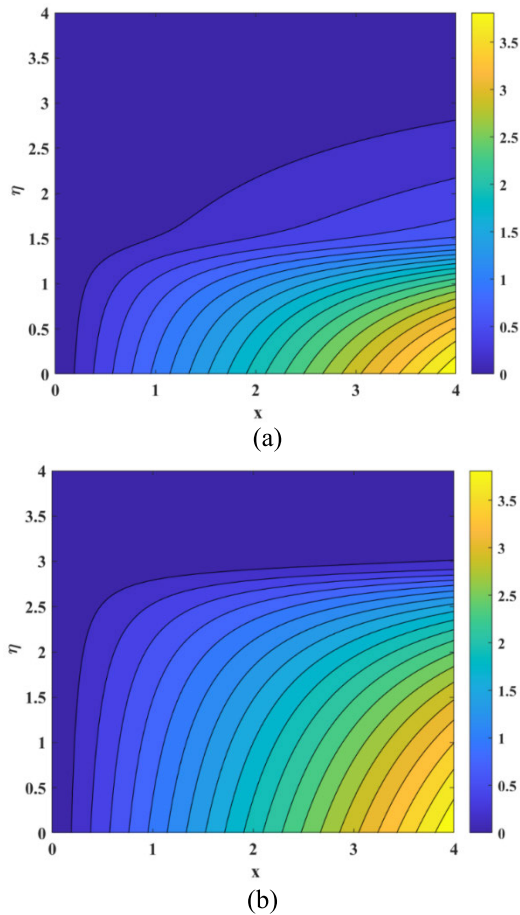
(a)

(b)

FIGURE 20. (a). Isothermal flow for $R_d = 0.2$. (b). Isothermal flow for $R_d = 1.2$.

TABLE 6. Analysis of $-\theta'(0)$ for Ag, MoS_2, and $Ag-MoS_2$.

Nt	Ag $(-\theta'(0))$	$MoS2 \, (-\theta'(0))$	$Ag-MoS_2$ $(-\theta'(0))$
0.1	1.33433718	1.42221003	1.64443005
0.3	1.33288700	1.41845170	1.6396390
0.5	1.3314662	1.41470446	1.63690668

Table 6 represents the reduced Nusselt number for the NF and HNF using dissimilar values of Thermophoresis parameter. It is observed that HNF has higher heat transmission rate as related to NF.

VI. CONCLUSION

A mathematical model is established to scrutinize the effect of Lorentz force, thermal radiation, joule heating, heat source and injection parameters, Brownian and thermoporetic diffusions on the hybrid nanofluid over the moving wedge. The stability exploration is reported for the existing study in order to confirm the stable solution which makes the novelty of

the study. The nanoparticles MoS_2 and Ag are suspended in ethylene glycol and water using as a host fluid. The numerical solution is obtained from the dimensionless first order differential equations which are gained from the basic flow equations through similarity transformations variables. The influences of emerging aspects on heat, velocity as well as concentration are revealed through graphs and tables. Since some factors exhibit multiple solutions, a stability evaluation is utilized for the stable solution. So, the novelty of the current study is to investigate the hybrid nanofluid flow and its stability.

The key points of the present study are:
1. It is reported that the point which connect the points of $\phi_{Ag} = 0.001, 0, 01$, and $\phi_{Ag} = 0.1$ are $M_{c1} = 0.5454$, $M_{c2} = 0.5035$, and $M_{c1} = 0.1716$, correspondingly.
2. It is worth mentioning here that SF boosts with rising magnitudes of ϕ_{Ag} in the stable solution however diminishing in the unstable solution.
3. The point which connects the stable and unstable solutions with respect to the ε and S are $\varepsilon_{c1} = 0.4995$, $\varepsilon_{c2} = -0.8920$, and $\varepsilon_{c3} = -2.8731$ regarding to the suction quantities $S = 0.5, 1.0$, and 1.5, respectively. It is investigated that the LSF and LNN are the escalating function of ε and S, in the stable branch but decreasing in the unstable branch.
4. It is interesting to note that as m is increased, the profiles of $f''(0)$ and $-\theta'(0)$ are sketched to be enhanced in the stable branch, which contributes excellent agreement with the results reported by Waini et al. [34]. This exploration demonstrations a 3.7% escalation in heat when m is boosted.
5. The distributions $\theta(\eta)$ and $f'(\eta)$ have a similar response when the parameter m increases while reverse behaviour is observed for $\phi(\eta)$.
6. When the Lewis number is higher, it makes the thermal and mass boundary layer regions smaller.
7. Direct relationship is established between the parameters Nt, Nb and dimensionless profiles $\theta(\eta)$, and $\phi(\eta)$.
8. When the radiation factor is improved, more heat is generated due to the radiation reaction in HNF which enhance the temperature inside the fluid.
9. It is publicized that as the values of R_d upsurges from $R_d = 0.2$ to $R_d = 1.2$, the isothermal flow also develops.

Future suggestion: This model relies entirely on a two-dimensional flow setup that incorporates traditional thermal and mass boundary situations, which slightly limits its applicability. However, if the exploration is to be conducted in a three-dimensional manner using the passive control approach and incorporating a convective heating or melting heat transmission development, it could prove to be convenient for engineering applications.

CONFLICT OF INTEREST

Authors declare that there is no conflict of interest regarding the publication of this article.

DATA AVAILABILITY STATEMENT

All data include in this manuscript

REFERENCES

[1] S. U.-S. Choi, "Nanofluid technology: Current status and future research," Argonne National Lab. (ANL), Argonne, IL, USA, 1998.

[2] J. C. Umavathi and A. J. Chamkha, "Convective stability of a permeable nanofluid inside a horizontal conduit: Fast chemical reactions," *Math. Comput. Simul.*, vol. 187, pp. 155–170, Sep. 2021.

[3] C. G. N. Ketchate, P. T. Kapen, D. Fokwa, and G. Tchuen, "Stability analysis of non-newtonian blood flow conveying hybrid magnetic nanoparticles as target drug delivery in presence of inclined magnetic field and thermal radiation: Application to therapy of cancer," *Informat. Med. Unlocked*, vol. 27, 2021, Art. no. 100800.

[4] V. Puneeth, M. Sarpabhushana, M. S. Anwar, E. H. Aly, and B. J. Gireesha, "Impact of bioconvection on the free stream flow of a pseudoplastic nanofluid past a rotating cone," *Heat Transf.*, vol. 51, no. 5, pp. 4544–4561, 2022.

[5] M. Irfan, P. Sunthrayuth, A. Ali Pasha, M. S. Anwar, and W. A. Khan, "Phenomena of thermo-sloutal time's relaxation in mixed convection Carreau fluid with heat sink/source," *Waves Random Complex Media*, pp. 1–13, Apr. 2022.

[6] Z. Hussain, Z. Bashir, and M. S. Anwar, "Analysis of nanofluid flow subject to velocity slip and Joule heating over a nonlinear stretching Riga plate with varying thickness," *Waves Random Complex Media*, pp. 1–17, Sep. 2022.

[7] M. Rafati, A. A. Hamidi, and M. Shariati Niaser, "Application of nanofluids in computer cooling systems (heat transfer performance of nanofluids)," *Appl. Thermal Eng.*, vols. 45–46, pp. 9–14, Dec. 2012.

[8] R. Razzaq and U. Farooq, "Non-similar forced convection analysis of Oldroyd-B fluid flow over an exponentially stretching surface," *Adv. Mech. Eng.*, vol. 13, no. 7, Jul. 2021, Art. no. 168781402110346.

[9] R. Razzaq, U. Farooq, J. Cui, and T. Muhammad, "Non-similar solution for magnetized flow of Maxwell nanofluid over an exponentially stretching surface," *Math. Problems Eng.*, vol. 2021, pp. 1–10, May 2021.

[10] J. Cui, S. Munir, S. F. Raies, U. Farooq, and R. Razzaq, "Non-similar aspects of heat generation in bioconvection from flat surface subjected to chemically reactive stagnation point flow of Oldroyd-B fluid," *Alexandria Eng. J.*, vol. 61, no. 7, pp. 5397–5411, Jul. 2022.

[11] A. H. Mahmoudi, I. Pop, M. Shahi, and F. Talebi, "MHD natural convection and entropy generation in a trapezoidal enclosure using Cu–water nanofluid," *Comput. Fluids*, vol. 72, pp. 46–62, Feb. 2013.

[12] F. Selimefendigil and H. F. Öztop, "Numerical study of MHD mixed convection in a nanofluid filled lid driven square enclosure with a rotating cylinder," *Int. J. Heat Mass Transf.*, vol. 78, pp. 741–754, Nov. 2014.

[13] H. F. Öztop, A. Sakhrieh, E. Abu-Nada, and K. Al-Salem, "Mixed convection of MHD flow in nanofluid filled and partially heated wavy walled lid-driven enclosure," *Int. Commun. Heat Mass Transf.*, vol. 86, pp. 42–51, Aug. 2017.

[14] A. Jan, M. Mushtaq, U. Farooq, and M. Hussain, "Nonsimilar analysis of magnetized Sisko nanofluid flow subjected to heat generation/absorption and viscous dissipation," *J. Magn. Magn. Mater.*, vol. 564, Dec. 2022, Art. no. 170153.

[15] S. Riaz, M. F. Afzaal, Z. Wang, A. Jan, and U. Farooq, "Numerical heat transfer of non-similar ternary hybrid nanofluid flow over linearly stretching surface," *Numer. Heat Transf., A, Appl.*, pp. 1–15, Sep. 2023.

[16] T. Hayat and S. Nadeem, "Heat transfer enhancement with Ag–CuO/water hybrid nanofluid," *Results Phys.*, vol. 7, pp. 2317–2324, Jan. 2017.

[17] S. S. U. Devi and S. P. A. Devi, "Numerical investigation of three-dimensional hybrid Cu–Al$_2$O$_3$/water nanofluid flow over a stretching sheet with effecting Lorentz force subject to Newtonian heating," *Can. J. Phys.*, vol. 94, no. 5, pp. 490–496, May 2016.

[18] A. J. Chamkha, A. Doostanidezfuli, E. Izadpanahi, and M. Ghalambaz, "Phase-change heat transfer of single/hybrid nanoparticles-enhanced phase-change materials over a heated horizontal cylinder confined in a square cavity," *Adv. Powder Technol.*, vol. 28, no. 2, pp. 385–397, Feb. 2017.

[19] S. Amala and B. Mahanthesh, "Hybrid nanofluid flow over a vertical rotating plate in the presence of Hall current, nonlinear convection and heat absorption," *J. Nanofluids*, vol. 7, no. 6, pp. 1138–1148, Dec. 2018.

[20] S. S. C. Ghadikolaei, "An enviroeconomic review of the solar PV cells cooling technology effect on the CO$_2$ emission reduction," *Sol. Energy*, vol. 216, pp. 468–492, Mar. 2021.

[21] S. S. C. Ghadikolaei, "Solar photovoltaic cells performance improvement by cooling technology: An overall review," *Int. J. Hydrogen Energy*, vol. 46, no. 18, pp. 10939–10972, Mar. 2021.

[22] S. S. Ghadikolaei and M. Gholinia, "3D mixed convection MHD flow of GO-MoS$_2$ hybrid nanoparticles in H$_2$O–(CH$_2$OH)$_2$ hybrid base fluid under the effect of H$_2$ bond," *Int. Commun. Heat Mass Transf.*, vol. 110, Jan. 2020, Art. no. 104371.

[23] S. S. Ghadikolaei and M. Gholinia, "Terrific effect of H$_2$ on 3D free convection MHD flow of C$_2$H$_6$O$_2$H$_2$O hybrid base fluid to dissolve Cu nanoparticles in a porous space considering the thermal radiation and nanoparticle shapes effects," *Int. J. Hydrogen Energy*, vol. 44, no. 31, pp. 17072–17083, Jun. 2019.

[24] S. S. Ghadikolaei, M. Gholinia, M. E. Hoseini, and D. D. Ganji, "Natural convection MHD flow due to MoS$_2$–Ag nanoparticles suspended in C$_2$H$_6$O$_2$H$_2$O hybrid base fluid with thermal radiation," *J. Taiwan Inst. Chem. Eng.*, vol. 97, pp. 12–23, Apr. 2019.

[25] G. Kumaran, R. Sivaraj, A. S. Reddy, B. R. Kumar, and V. R. Prasad, "Hydromagnetic forced convective flow of carreau nanofluid over a wedge/plate/stagnation of the plate," *Eur. Phys. J. Special Topics*, vol. 228, no. 12, pp. 2647–2659, Dec. 2019.

[26] P. Sudhagar, P. K. Kameswaran, and B. R. Kumar, "Non-Darcy effects on mixed convective nanofluid over a wedge in a porous medium," *J. Porous Media*, vol. 21, no. 9, pp. 781–791, 2018.

[27] S. A. Gaffar, V. R. Prasad, B. R. Kumar, and O. A. Beg, "Computational modelling and solutions for mixed convection boundary layer flows of nanofluid from a non-isothermal wedge," *J. Nanofluids*, vol. 7, no. 5, pp. 1024–1032, Oct. 2018.

[28] C. M. Mohana and B. R. Kumar, "Shape effects of Darcy–Forchheimer unsteady three-dimensional CdTe-C/H$_2$O hybrid nanofluid flow over a stretching sheet with convective heat transfer," *Phys. Fluids*, vol. 35, no. 9, Sep. 2023, Art. no. 092002.

[29] K. Padmaja and B. R. Kumar, "Viscous dissipation and chemical reaction effects on MHD nanofluid flow over a vertical plate in a rotating system," *ZAMM-J. Appl. Math. Mechanics/Zeitschrift Für Angewandte Mathematik Und Mechanik*, vol. 103, no. 9, 2023, Art. no. e202200471.

[30] D. R. Hartree, "On an equation occurring in Falkner and Skan's approximate treatment of the equations of the boundary layer," in *Mathematical Proceedings of the Cambridge Philosophical Society*, vol. 33, no. 2. Cambridge, U.K.: Cambridge Univ. Press, 1937, pp. 223–239.

[31] N. A. Yacob, A. Ishak, R. Nazar, and I. Pop, "Falkner–Skan problem for a static and moving wedge with prescribed surface heat flux in a nanofluid," *Int. Commun. Heat Mass Transf.*, vol. 38, no. 2, pp. 149–153, Feb. 2011.

[32] M. S. Alam, M. Ali, M. A. Alim, M. J. H. Munshi, and M. Z. U. Chowdhury, "Solution of Falkner- skan unsteady MHD boundary layer flow and heat transfer past a moving porous wedge in a nanofluid," *Proc. Eng.*, vol. 194, pp. 414–420, Jan. 2017.

[33] J. H. Merkin, "Mixed convection boundary layer flow on a vertical surface in a saturated porous medium," *J. Eng. Math.*, vol. 14, no. 4, pp. 301–313, Oct. 1980.

[34] P. D. Weidman, D. G. Kubitschek, and A. M. J. Davis, "The effect of transpiration on self-similar boundary layer flow over moving surfaces," *Int. J. Eng. Sci.*, vol. 44, nos. 11–12, pp. 730–737, Jul. 2006.

[35] I. Waini, A. Ishak, and I. Pop, "MHD flow and heat transfer of a hybrid nanofluid past a permeable stretching/shrinking wedge," *Appl. Math. Mech.*, vol. 41, no. 3, pp. 507–520, Mar. 2020.

[36] M. S. Anwar, M. Irfan, M. Hussain, T. Muhammad, and Z. Hussai, "Heat transfer in a fractional nanofluid flow through a permeable medium," *Math. Problems Eng.*, vol. 2022, pp. 1–18, Mar. 2022.

[37] R. Baby, V. Puneeth, S. S. Narayan, M. I. Khan, M. S. Anwar, O. T. Bafakeeh, M. Oreijah, and K. Geudri, "The impact of slip mechanisms on the flow of hybrid nanofluid past a wedge subjected to thermal and solutal stratification," *Int. J. Modern Phys. B*, vol. 37, no. 15, Jun. 2023, Art. no. 2350145.

[38] S. O. Alharbi, F. Smarandache, A. M. Elsiddieg, A. M. Alqahtani, M. R. Khan, V. Puneeth, and N. Becheikh, "The computational model of nanofluid considering heat transfer and entropy generation across a curved and flat surface," *Sci. Rep.*, vol. 13, no. 1, 2023, Art. no. 20059.

[39] V. Christianto and F. Smarandache, "Modeling virus as elastic sphere in Newtonian fluid based on 3D Navier–Stokes equations," *J Nanosci Nanomed*, vol. 2, no. 1, pp. 1–2, 2018.

[40] T. Watanabe, "Thermal boundary layers over a wedge with uniform suction or injection in forced flow," *Acta Mech.*, vol. 83, Sep. 1990, Art. no. 119e126.

AISHA M. ALQAHTANI received the Bachelor of Sciences degree (Hons.) in mathematics from Umm Al-Qura University, Mecca, Saudi Arabia, the M.Sc. degree (Hons.) in applied mathematics from Princess Nourah bint Abdulrahman University, Riyadh, Saudi Arabia, and the Ph.D. degree in applied mathematics from Heriot-Watt University, Edinburgh, Scotland, U.K. She is currently an Associate Professor in applied mathematics with the Mathematical Sciences Department, Princess Nourah bint Abdulrahman University. Her research interests include heat transfer, pours media, nanofluids, electro hydrodynamic, and magnetohydrodynamic.

ZEESHAN received the M.Sc. and M.Phil. degrees from Quaid-e-Azam University, Islamabad, and the Ph.D. degree from Abdul Wali Khan university, Mardan, Khyber Pakhtunkhwa, Pakistan. He is currently an Assistant Professor in mathematics with Bacha Khan University Charsadda, Khyber Pakhtunkhwa. He has published 90 articles in good impact factor journals and has participated in national conferences. His research interests include magnetohydrodynamic, nano fluid, heat transfer, hall effect, electrohydrodynamic, thin film, and heat exchangers.

WARIS KHAN received the M.Sc. degree from Quaid-e-Azam University, Islamabad, Pakistan, the M.S. degree from COMSATS University Abbottabad, Khyber Pakhtunkhwa, Pakistan, and the Ph.D. degree from the Islamia College University, Peshawar, Khyber Pakhtunkhwa. He is currently a Lecturer in mathematics with Hazara University Mansehra, Khyber Pakhtunkhwa. He has a prolific academic record with 94 articles published in high-impact factor journals, along with active participation in national conferences. His research interests include magnetohydrodynamics, nanofluids, heat transfer, hall effect, electrohydrodynamics, thin films, and heat exchangers.

FLORENTIN SMARANDACHE received the M.Sc. degree in mathematics and in computer science from the University of Craiova, Romania, and the Ph.D. degree in mathematics from the State University of Kishinev. He completed his postdoctoral research in applied mathematics from Okayama University of Sciences, Japan, and The Guangdong University of Technology, Guangzhou, China. He is currently an Emeritus Professor in mathematics with The University of New Mexico, USA. He has been the Founder of Neutrosophy (generalization of dialectics), neutrosophic set, logic, probability, and statistics, since 1995, and has published 100's of papers and books on neutrosophic physics, superluminal and instantaneous physics, unmatter, quantum paradoxes, absolute theory of relativity, redshift and blueshift due to the medium gradient and refraction index besides the Doppler effect, paradoxism, outerart, neutrosophy as a new branch of philosophy, law of included multiple-middle, multispace and multistructure, HyperSoft set, TreeSoft set, IndetermSoft set and IndetermHyperSoft set, SuperHyperGraph, SuperHyperTopology, SuperHyperAlgebra, SuperHyperFunction, Neutrosophic SuperHyperAlgebra, degree of dependence and independence between neutrosophic components, refined neutrosophic set, neutrosophic over-under-off-set, plithogenic set/logic/probability/statistics, symbolic plithogenic algebraic structures, neutrosophic triplet and duplet structures, quadruple neutrosophic structures, extension of algebraic structures to NeutroAlgebra and AntiAlgebra, NeutroGeometry and AntiGeometry, NeutroTopology and AntiTopology, refined neutrosophic topology, refined neutrosophic crisp topology, and dezert-smarandache theory to many peer-reviewed international journals and many books. He presented papers and plenary lectures to many international conferences around the world. In addition, he has published many books of poetry, dramas, children stories, translations, essays, a novel, folklore collections, traveling memories, and art albums. For more information visit the link (http://fs.unm.edu/FlorentinSmarandache.html).
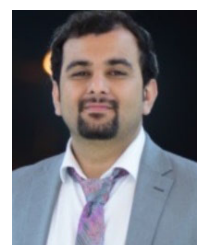
NIDHAL BECHEIKH is currently an Assistant Professor with the Department of Chemical and Materials Engineering, Northern Border University, brings over ten years of extensive experience to the dynamic field of chemical engineering. His expertise is covering essential subjects from thermodynamics and kinetics to advanced fluid mechanics, with a particular focus on the critical aspects of modeling and simulation for engineering processes. In the academic research, he has made notable contributions to the study of micro-structured reactors and delving into the intricacies of mass transfer limitations in photocatalytic processes. His work in this area is addressing some of the fundamental challenges in reaction engineering and offering innovative solutions that enhance efficiency and sustainability.

ROOBAEA ALROOBAEA received the bachelor's degree (Hons.) in computer science from King Abdulaziz University (KAU), Saudi Arabia, in 2008, and the master's degree in information system and the Ph.D. degree in computer science from the University of East Anglia, U.K., in 2012 and 2016, respectively. He is currently an Associate Professor with the College of Computers and Information Technology, Taif University, Saudi Arabia. His research interests include human–computer interaction, software engendering, cloud computing, the Internet of Things, artificial intelligent, and machine learning.

TASEER MUHAMMAD is currently an Assistant Professor with the Department of Mathematics, King Khalid University, Abha, Saudi Arabia. His research interests include fluid mechanics, series and numerical solutions of ODEs and PDEs, and applied mathematics.

• • •